

Research Article

Potential Consequence of Interconnected Intervention against Systemic Risk (COVID-19) via a Model-Driven Network-Agent Dynamic

Chulwook Park ^{1,2,3}

¹International Institute for Applied Systems Analysis (IIASA), Laxenburg 2361, Austria

²Okinawa Institute of Science and Technology (OIST), Okinawa 1919-1, Japan

³Department of Physical Science, Seoul National University, Seoul 08826, Republic of Korea

Correspondence should be addressed to Chulwook Park; pcw8531@gmail.com

Received 29 November 2021; Revised 30 April 2022; Accepted 11 June 2022; Published 30 November 2022

Academic Editor: Francesco Lo Iudice

Copyright © 2022 Chulwook Park. This is an open access article distributed under the Creative Commons Attribution License, which permits unrestricted use, distribution, and reproduction in any medium, provided the original work is properly cited.

This study estimates the consequences of risk propagation, such as that of COVID-19, using network-agent dynamics. Given several scenarios, the network-agent model provides critical insights into infection risk using a model-driven approach to interconnected interventions. The simulation results suggest that employing a nonevolutionary governing structure with evolutionary individual interaction parameters guided by testing can help suppress outbreaks to levels below the standard critical-care capacity. Furthermore, setting the protection level as the macroscale and the shrinking of individual interactions as the microscale, the effects of social distancing on transmission rates are reflected in the disease model. In addition, the parameters that reflect the best feasible scenarios can be determined. These findings are relevant to COVID-19 pandemic policies wherein interconnected interventions reduce the socioeconomic costs of risk propagation.

1. Introduction

Pandemic contagions spread following the general principle of exponential growth [1]. Hence, as each agent is infected, risk propagation at least doubles. Although, initially, the cases increase slowly, an entire population can be infected within a few days [2]. Socioeconomically, COVID-19 (i.e., a systemic risk) has wreaked catastrophic global damage since early 2020. The impact has driven fundamental social changes across the globe [3]. To understand how these effects occur and better identify them, their essential properties and structures have been widely investigated [4].

When an entire population is negatively affected, systemic failure of treatment and intervention is bound to occur [5]. Numerous studies have scrutinized this in terms of biology, finance, medicine, and so on. Because various risks propagate differently, the entire extent of any risk must be well-gauged to mitigate it effectively. Hence, progress has been made in using suitable approaches [6]. Recent studies have offered clear recommendations about observed changes

in risk phenomena [7]. Ideally, despite risks being immutable, they are mitigated and suppressed by the various interventions applied [8, 9]. To elaborate on this argument, we consider the common interventions employed by several countries.

1.1. Lockdown. Many studies have focused on the socioeconomic impact of COVID-19 [10]. Big data have been used to measure the percentage change in the propagation patterns (i.e., community mobility) [11]. Consequently, certain countries imposed quarantines, which reduced transmission by ~90%. Others closed their borders to establish nationwide lockdowns [12]. However, many of these lockdowns were partially relaxed and later lifted prior to the risk being fully controlled. Mobility returned to normal in many places, and risk mitigation was relegated to individual choice [13]. Some countries imposed no lockdowns, and their mobility still decreased for similar reasons. Schools, cafes, restaurants, and shops remained open to avoid greatly

disrupting the economy [14], and stay-at-home policies were only a recommendation. Nevertheless, citizens voluntarily reduced their mobility by 10–20% from the global baseline.

This raises questions about best-case scenarios. Countries that implemented strict lockdowns and experienced considerable socioeconomic losses recovered and now exhibit nearly normal patterns. Conversely, some countries that implemented strict lockdowns saw huge decreases in socioeconomic status and have not recovered [15]. Some countries did not impose strict restrictions, and they still suffer greatly. Other countries employed various responses based on their stronger socioeconomic status and fared consistently better, which implies that they have now also largely returned to normal [16].

1.2. Herd Immunity. Another strategy suggests that herd immunity can be acquired against a pandemic, first causing the exponential infection rate to flatten, followed by a steady drop [17]. Unfortunately, herd immunity does not apply well to scenarios in which the pathogen or virus mutates, resulting in new infectious strains. We investigate this further in this paper [18]. Herd immunity theoretically protects a considerable number of vulnerable people (e.g., children) from diseases [17, 18], and ostensibly, it should allow the global economy to reopen safely; some believe that it will ultimately result in an end to pandemics. However, the path to herd immunity includes significant hurdles, and experts suggest that it can take years to achieve.

Widespread infections and vaccinations [19] are two scientific approaches to reaching herd immunity. Experts estimate that fewer than 5% of people worldwide have contracted COVID-19 [20]. To reach herd immunity, that number would have to be 60–70%. For this, more than 4 billion people would have to be infected. This would result in tens of millions of people dying and hundreds of millions becoming gravely ill [19]. This would devastate global economies. Moreover, it is entirely unnecessary. Furthermore, there is no guarantee that a broad infection would lead to eradication. We do not have many examples to explore of complete immunity arising from natural conditions because the population continues to increase exponentially [21]. Thus, all new offspring remain susceptible to infection.

1.3. Vaccines. Experts suggest that a more efficient approach to immunity is through vaccination [22]. This is how scientists (nearly) eradicated smallpox. Because of vaccines, childhood mortality has dropped dramatically for decades. Experts may not yet have sufficient information about COVID-19 to predict the likelihood of reaching herd immunity [23], and there are considerable barriers to achieving that goal. Even with a vaccine, scientists are unsure of how long the natural immunity may last [22]. There is a large difference between a 6-month immunity and being protected for 10+ years. For other known respiratory viruses (e.g., influenza), antibodies tend to weaken over time. Scientists have already observed this in patients recovering from COVID-19; thus, it remains unclear how long the COVID-19 vaccine will remain effective, and the period of

effectiveness will be measured in months or years instead of lifetimes [23]. Another challenge is that because not all vaccines work in the same manner (i.e., new COVID variant), their effectiveness will differ [24].

As cases surge worldwide, some experts are optimistic [25]. According to a recent vaccination report [26], it is estimated that the number of infected people could be reduced if the inoculation rates were fast enough, notwithstanding each vaccine's efficacy. Scientists have shown that the reproduction index is not fixed, and it is constantly refined by examining past experiences (i.e., Middle East Respiratory Syndrome (MERS)). This is similar to current COVID-19 mutations. The reproductive index is very likely to repeat an increasing/decreasing pattern that includes infections after vaccinations [27]. Thus, health experts continue to recommend imposing appropriate interventions and measures at interconnected macro- and microscales to slow the spread [24, 27]. Hence, it is necessary to continue rigorous controls [26]. More importantly, individuals with a tendency to maintain safe distancing from others and remaining isolated have a better chance of survival [25].

1.4. Gab Statement. Although the abovementioned assumptions can help achieve anticontagion performance, detailed investigations of COVID-19 are still necessary [28]. The future requires combining large repositories of data to predict trajectories that will provide realistic options [29]. Therefore, a computerized individualized model may serve as an essential tool that combines real circumstances with simulations [30]. The results can be regarded as a sampled subset of the underlying social network [31]. For example, if a plausible model of the underlying network and its agent dynamics are found, we may be able to infer which contacts are likely to create a propagation route [32]. Indeed, communication among nearby individuals is usually more frequent than for long-range connections, thereby providing efficient paths for viral spreading, as observed in small-world networks. Furthermore, the mechanisms and serial algorithms that underpin our understanding of risk propagation by networked agents must be evaluated [33] to help us identify common grounds for integrating knowledge and strategies. We may then agree on definitions and reconcile the approaches adopted in multiple fields for an interdisciplinary study of systemic risks.

1.5. Purpose. The purpose of this research is to analyze the potential consequences of risk propagation because pathogens play an integral role in regulating infection. In particular, by incorporating detailed macroscales (nonevolutionary) and microscales (evolutionary) of real-world network mechanisms (see the Materials and Methods section) [34], insightful information can be gained for a network-agent simulation to estimate parameter ranges from an extended disease model for susceptible, exposed, infectious, and recoverable (SEIR) simulation. The advantage of this combined approach is its flexibility. Hence, we extend certain prototypical results of the disease model (e.g., population dynamics) into more realistic simulations (e.g., agent-based dynamics) that fully consider these potential

consequences under the assumption that most people would follow a reliable strategy for a long period.

1.6. Value. Pandemic risks are a significant concern in many countries, and they have been widely examined in various fields [35, 36] because there are no specific therapeutics licensed for treating the disease [37]. To understand the risk potential, we suggest intervention via appropriate contemporary dynamic model studies. Some results consider a direct relationship between infection risk and the level of intervention for mitigation. From this, a significant opportunity arises from which we can produce mitigating strategies to transform an entire population's systemic risk.

2. Materials and Methods

Risk is a property of system interconnectivity, and it can be described in terms of system instability, which is caused or exacerbated by idiosyncratic events that result in a potential catastrophe [38]. In particular, a connectivity pattern is a key to understanding risk and how elements of a framework communicate with each other [39]. Thus, it has been suggested that a strategic decision process can be used to explore the influence of networked interaction among agents [40] and understand the architecture of artificial systems from the network-property perspective [41, 42]. In this paper, we develop a model for these processes with reference to the COVID-19 pandemic and its propagation. The following model specification builds on an agent-based model of systemic risk with evolving strategies determining protective investments against cascading failures that has been originally developed by Ulf Dieckmann and analyzed together with Chulwook Park at the International Institute for Applied Systems Analysis (IIASA), Austria.

2.1. Network Property. Many empirical graphs are modeled on small-world networks (e.g., Facebook and Wikipedia) [43]. There are individuals (nodes) and neighbors per node that denote the number of links, some of which can be rewired. Essentially, they can be attached to distant neighbors to model wide-area connections [44]. The small-world aspect of our network model allows for a relatively efficient set of links that do not require many decentralized resources to maintain connectivity (see Supplementary Materials I for more details of the basic network property). This represents a range of degrees of distribution (random \leftarrow \rightarrow regular) (Figure 1). For example, we can infer from the structure which social contacts are favored as the infection route. Naturally, contacts between nearby people are usually more frequent than long-range connections, providing efficient routes for a virus to spread, as described by a small-world network. The level of connectivity between a typical node and a local hub can be significant; however, it is not notably high. Hence, we can form network properties to help focus our analysis.

2.2. Operating Mechanisms. An operating network has a small-world appearance, and a relationship holds between

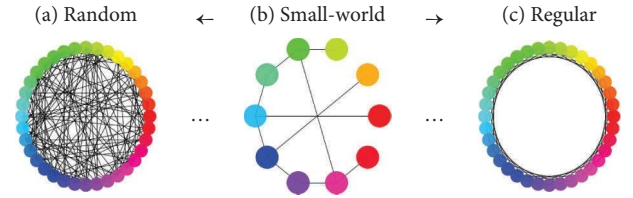


FIGURE 1: Prototype of the small-world network structure. (a) The random network. (b) The small-world network structure defined by ten nodes, two connections at each node, and the probability of rewiring $\beta=0.2$. (c) The regular network structure.

the vertices (nodes) and the edges (lines). Hence, a mechanism is obtained as (Tables 1 and 2)

$$A = G[n, p, \beta], p \in (0, 1), \beta \in (0, 1) \longrightarrow Am \times n. \quad (1)$$

Any node (n) can be linked to any other node. Because the collection of nodes influences the probability of connections ($p \in (0, 1)$), our model investigates the distribution of network connections (i.e., degree probability). Additionally, network rewiring ($\beta \in (0, 1)$) will have unpredictable effects in relation to individual ties because this allows for different approaches to diverse risks (i.e., mobility and migration). This is because the nodes influence each other in the same way as originating strategies and distributed security (e.g., firms, banks, food webs, supply chains, and germs).

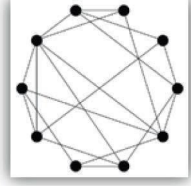
2.3. Individual Property. To observe the propagation process, the corresponding network-agent evolutionary dynamics [45] model uses an array (vector) to represent the probability of infection, $p \in (0, 1]$, with a given set of influenced nodes ($1 \leq j \leq N$), denoted by (p_j) . Each node can persist in one of two states: uninfected or infected. All nodes initially exist without infection.

The matrix no longer represents the adjacency matrix (A). It continues to be labeled as rows and columns with values of one and zero; the key difference is the possibility of showing each node's state (1 = infection; 0 = absence of infection) based on the time step (see Figure 2).

2.4. Immunodynamics as Antibodies to the Virus. With the fundamental model characteristics, we stipulate that an elementary level of risk (i.e., cascades of infection) depends on the cooccurrence of the i and j nodes. In these dynamics, an agent is associated with each node and characterized by its immunity and strategy (the strategy values f_{p0} and f_{p1} evolve through social learning and strategy exploration; see section (vi) for more details). For each time step, each agent receives one unit of immunity, which is added to that agent's immune capacity, c , for which the fractions f_m and f_p are spent on maintenance and protection, respectively. Thus, the capacity value is updated to $1 + (1 - f_m - f_p)c$.

2.5. Susceptible Dynamics (Basic Transmission Rate as the Number of Individuals Infected by One Individual). Virus infection potential can originate at each node with a

TABLE 1: Small-world network property.

Definition	Parameter	Range	Created small-world network (example)
Number of individuals	n	$\in (0, \infty)$	
Connection probability	p	$\in (0, 1)$	
Rewiring probability	β	$\in (0, 1)$	
Linear dimension (matrix)	$m * n$	row, col	

* Three parameters. n : number of nodes. p : number of edges for a new node to attach to. β : rewiring probability to the edge.

TABLE 2: Code example of small-world network.

```
[In] # import modules
import networkx
import matplotlib.pyplot as plt

[In] # create object
G = networkx.watts_strogatz_graph(n = 10, p = 4, beta = 0.2)
pos = networkx.circular_layout(G)

[In] # illustrate graph
networkx.draw_networkx(G, pos, node_color = 'k', node_size = 500)
```

probability, $p_n \in [0, 1]$, and it can propagate along each link with a probability, $p_l \in [0, 1]$, at each time step. This rate reflects the transmission rate (β_t), which is the average number of individuals infected by one individual in a susceptible population. When this value is larger than one (i.e., $\beta_t > 1$), it means that one infected individual transmits the disease or virus to two others (i.e., $p_l > 1$), and the virus spreads exponentially. However, if this rate is less than one (i.e., $\beta_t < 1$), the number of new infections decreases (i.e., $p_l < 0.1$).

To match this contextual spreading mechanism, let us denote the number and fraction of failed agents by N_f and f , respectively, and consider two successive steps t and $t + 1$. Suppose that, at time t , there are N_f and $N - N_f$ failed and not failed nodes, respectively. Therefore, the number of not failed nodes at $t + 1$ is $N_f + p_p(N - N_f)$, and the number of failed nodes is $N_f = (1 - p_p)(N - N_f)$, $f = (1 - p_p/2 - p_p)$. Here, p_p is the average protection probability among not failed nodes. The above relation shows that the value of f

is a decreasing function of p_p . For $p_p = 1$ (i.e., full protection), there will be no failed agents. We modified the propagation probability, p_l , because p_p will need to be replaced by $p_p = 1 - (1 - p_p)1 - (1 - p_l)^{(N_f)}$. This equation implicitly leads to $f = 1 - (1/(N p_l (1 - p_p)))$.

This rate gives us an idea of how quickly the infection spreads from one individual (p_n) to the next (i.e., the basic reproduction number: COVID-19 is estimated to be between 2 and 4). Thus, we apply this rate to COVID-19 and embed these potential infections that become infections with a probability of $1 - p_p$, depending on the agent's investment in protection. Hence, a possible choice is

$$P_p = \frac{P_{p,\max}}{(1 + c_{p,(1/2)} / (f_p c))}. \quad (2)$$

Here, $p_{p,\max}$ denotes the designated protection maximum. $c_{p,(1/2)}$ denotes an allocated reference (in units of $c_{p,(1/2)}$: simplifies the protection probability as $p_p = (p_{p,\max} / (1 + (1/(f_p c))))$, and $f_p c$ represents an evolutionary protection level multiplied by the updated immune capacity. The infection lasts for one time step (default), resulting in the loss of an agent's immune capacity. For those strategies, each agent chooses its protection level according to the heuristic:

$$f_p = f_{p0} + f_{p1}C, \quad (3)$$

truncated to the interval $(0, 1 - f_m)$:

$$\vec{v} \rightarrow \vec{f} \rightarrow f(\vec{v}), f(\vec{v}) = \begin{cases} 0 < f(\vec{v}) < 0.9, & f_m = 0.9, \\ 0 < f(\vec{v}) < 0.1, & f_m = 0.1, \end{cases} \vec{v}|_{f_p = f_{p0} + f_{p1}C}. \quad (4)$$

For the initialization of strategy values, two arrays are added for vectorization:

$$f_{p0} = \vec{w}_i, f_{p1}C = C\vec{w}_i, \quad (5)$$

where \vec{w}_{i1} denotes the vectorization as the designated strategy of (f_{p0}). \vec{w}_{i2} represents a vectorization as the designated strategy of (f_{p1}) multiplied by the eigenvector centrality from the graph (C), which indicates the

centrality of the agent's node, as normalized to the interval $(0, 1)$:

The eigenvector centrality (C) for node i is ($Ax = \lambda x$), where the matrix denotes the network with eigenvalue λ .

2.6. Strategy Dynamics (as a Social Interaction). The strategy values, f_{p0} and f_{p1} , evolve through social learning and strategy exploration, reflecting the individual interaction

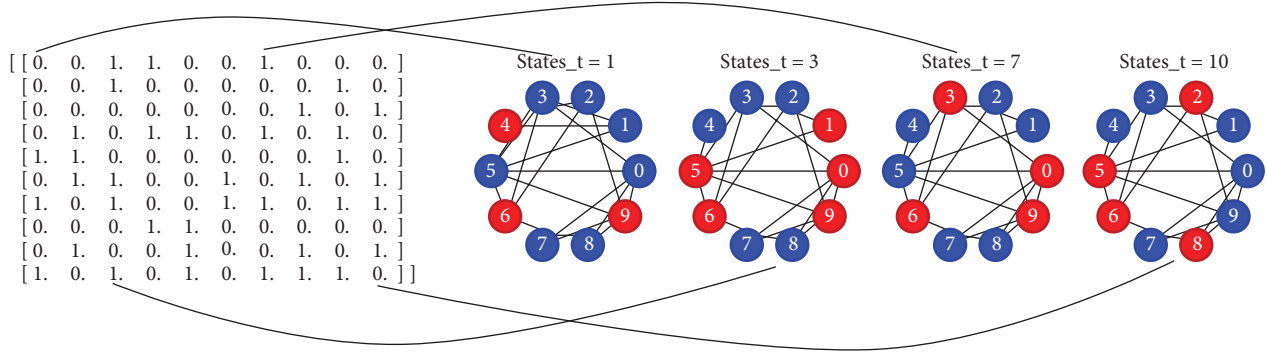


FIGURE 2: Visualization of a virus propagating over time. Right plot shows the individuals' (0–9) state from the absence of infection (blue) to infection (red) with their connections (lines). The matrix on the left denotes the time series (horizontal axis $t1-t10$) of the individual's state (vertical axis 1 = infection; 0 = absence of infection). The lines between the matrix and the networks indicate their relationship corresponding to its state at the time. Nodes = 10; connection $p = 0.5$; and rewiring $p = 0.5$.

during COVID-19 as follows: At each time step, each agent randomly chooses another as a role model with probability $p_r \in [0, 1]$ and imitates that agent's strategy values with the probability,

$$p_i = [1 + \exp(-\omega \Delta \pi)]^{-1}, \pi_r - \pi_f = \Delta \pi |_{\pi_r = \text{rolemodel}}, \quad (6)$$

where p_i denotes the probability of the role model being accepted for imitation, π_f represents the immune capacity of the focal individual, π_r denotes the immune capacity of the role individual, "exp" denotes the exponential, and ω represents the intensity of the selection ($\omega < 1$ = weak selection, $\omega \rightarrow \infty$ = strong selection). The focal individual imitates the nearby role individual's strategy, comparing its new immunity (large $\Delta \pi$ = large immune capacity difference; small $\Delta \pi$ = small immune capacity difference). Then, the focal individual chooses to imitate the strategy of the role individual (see Table 3 (code book) for the details of the mechanism).

Additionally, at each time step, each agent having a probability of $p_e \in [0, 1]$ randomly chooses one of its two strategy values and alters it with a normally distributed increment with a mean of zero and a standard deviation

$$\sigma_e | f(x|\mu, \sigma^2) = \frac{1}{\sqrt{2\pi\sigma^2}} \exp\left(-\frac{(x-\mu)^2}{2\sigma^2}\right) | \mu \in R, \sigma^2 > 0, \quad (7)$$

where x denotes individual immunity, μ represents the mean (location), and σ^2 denotes the variance (square scale) (see Table 4 (code book) for the detail of the mechanism).

2.7. Recovery Dynamics (Delay of Isolation and Quarantine). Given a recovery which, in this context, refers to the fraction of recovered individuals having immunity, this function (or infection) lasts for one time step and results in the loss of an agent's immunity according to the reset virus infection potential:

$$\text{random}(n) < r_t = 1 \rightarrow 1 - p_p = 0, \quad (8)$$

where $\text{random}(n) < \text{rec} = 1$ denotes randomly chosen individuals having a certain probability ($\text{random}(n)$) and the infectious potential of any individual is $(1 - p_p)$, which is selected based on a certain probability that approaches zero. At the end of each time step, all failed agents will recover.

$$t_r \in [0, \infty], t_r < 1 = \text{strong intervention}, t_r \rightarrow \infty = \text{weak intervention}. \quad (9)$$

By default, this recovery rate is implemented by resetting the infectious potential after every $r_t = 1$ time steps. Simultaneously, to control this intervention, we allowed the number of time steps to be controlled by another parameter ($t_r \in [0, \infty]$), which represents the delay of social distancing, infected isolation, and quarantine (until recovered) as the recovery time delay. The parameterization of these macrovariables (t_r) and microvariables (r_t) is designed to provide insight into the more realistic conditions for recovery from the virus and the more sophisticated recovery mechanisms.

3. Performance Evaluation (Including Interpretation of the Results)

3.1. Assumption of the Network-Agent Dynamic from the Disease (SEIR) Dynamic. First, we assume a risk potential (virus) that is represented by the COVID-19 basic reproductive number (R_t) [46] to the network-agent dynamic's number of infections ($f_n \leftarrow p_n \in [0, 1], p_l \in [0, 1]$). This epidemiological term can be derived from the average number of new offspring generated by each influenced individual and reflects the transmission rate (β_t). Differently

TABLE 3: Code example of the strategy dynamics (imitation).

for i in range (n):	# loop for every individual within the t loop
#-----	
# imitation	
#=====	
R1 = np.random.random()	# randomly choose a certain (%) only 1 time
if R1 <= pr:	# conditional
ff = i	# focal individual (each node i)
while True:	# it is true
rr = np.random.choice (n)	# randomly choose role individual
if ff != rr:	# until focal choose a different role individual
break	# exit out of the loop
pi = 1/(1 + (np.exp (-s * (B[rr,0]-B[ff,0])))	# calculate (Fermi) function
R2 = np.random.random()	# randomly choose a certain (%) only 1 time
if R2 <= pi:	# conditional
temp[ff, 1:3] = B[rr,1:3]	# imitate the role individual
B[:, 1:3] = temp[:, 1:3]	# update strategy values

TABLE 4: Code example of the strategy dynamics (exploration).

for i in range (n):	# loop for every individual within the t loop
#-----	
# exploration	
#=====	
temp = B[:,1:3]	# a temporary variable to save strategies
R3 = np.random.random(size = [n, 2]) <= (0.5 * pe)	# randomly choose a certain(%) with conditional
temp [R3] += np.random.normal (mu, sigma, size = [n,2])[R3]	# normally distributed increment
B[:,1:3] = temp	# update strategy values

expressed, the number of people currently infected in a region and the percentage of new infections are given. A high value implies that it propagates easily, and a low value indicates resistance. The critical assumption here is that everyone is susceptible; no one is excluded.

There are three basic scenarios for the number of infections (f_n), which matches the reproductive number (R_t). It can be less than one, meaning that the number of new cases will decrease over time; it can also be equal to one, meaning that the case number is stable over time; or it can be greater than one, meaning that the infection is self-sustaining unless control measures are implemented. When the infectious potential ($f = 1 - (1/(Np_t(1 - p_p)))$) influenced by this model's mechanism equals 1, one individual transmits the disease to another. These individuals will infect others either in a pessimistic-case scenario or in an optimistic-case scenario. Thus, the number of infected cases remains stable over time. If the infectious potential or reproduction number is less than one, then $R_t < 1 = f_n < 1$. Thus, over time the number of cases will decrease and will be dominated by the absence of infection, which is the ideal outcome. When the infectious potential or reproduction number is greater than one ($R_t > 1 = f_n > 1$), the protection equals 0.1. Hence, when each individual infects another (more than one) and the newly infected individuals then infect others (more than one), the number of infections increases exponentially over time (see Figure 3).

For the potential simulation (Figure 3), the population is set to N , which we have applied to South Korea (2019; 51.64 million); the results are represented as fractions of the population [45]. At each moment, the population is divided

into four categories that add to a total of 1 ($S =$ susceptible, $E =$ exposed, $I =$ infected, and $R =$ recovered (or dead), as inspired by the disease model), which indicates fractions of the population that evolve as follows:

$$\frac{dS}{dt} = \beta_t \frac{S_t}{N} I_t, \frac{dE}{dt} = \beta_t \frac{S_t}{N} I_t - \sigma E_t, \frac{dI}{dt} = \sigma E_t - \gamma I_t, \frac{dR}{dt} = \gamma I_t, \quad (10)$$

where parameter γ can be used for the rate per day at which an infected individual either infects or does not infect at a fixed parameter. For example, the COVID-19 case ($\gamma = 1/18$) reflects the estimated duration of the influence over 18 days [47]. The parameter σ represents the rate at which those exposed to the virus become infected; furthermore, it is considered a fixed parameter ($\sigma = (1/4)$) to reflect the estimated incubation period. Thus, COVID-19 has an incubation period of 4 days in South Korea [48]. Here, β_t is the transmission rate, similar to the infectious potential defined by $Np_t \leftarrow p_t \in [0, 1]$ in the network-agent simulation. Of the people infected, a fraction S/N is susceptible. Thus, the transition occurs upon exposure. The parameter governing the rate of infection varies over time (see Supplementary Materials II for more details of the SEIR Model mechanism).

3.2. Part 1: Nonevolutionary Scale Effect with Rewiring. Based on the aforementioned premise, a protection dynamic can be implemented against the spreading virus. The network-agent dynamic model allows an agent to make a costly investment for protection. We assume that the risk is the

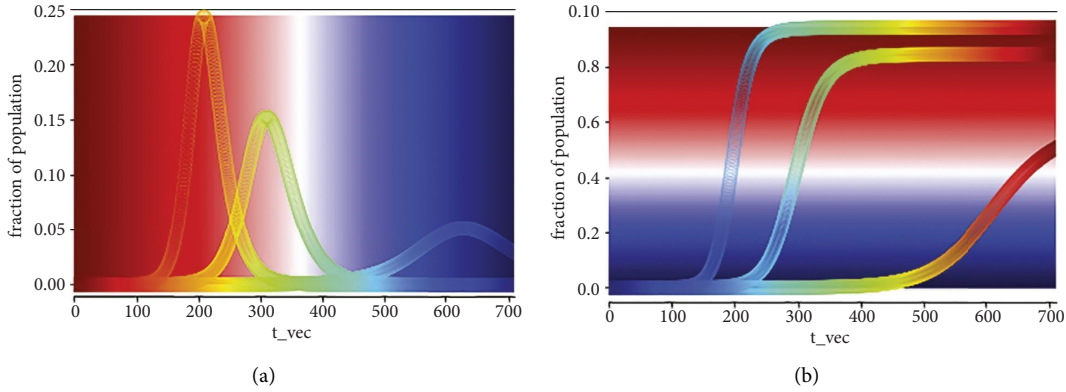


FIGURE 3: Simulation with the intervention scenario parameterized by reproduction number (R_t) = number of infections = f_n . (a) The fraction of the population (left: $R_t = 3.0$; middle: $R_t = 2.2$; right: $R_t = 1.5$) produced by the population dynamic model. (b) The cumulative cases as a fraction of the population (left: infectious potential (f_n) = high \leftarrow \rightarrow right: infectious potential (f_n) = low) produced by the network-agent dynamic model with the time step $t = 2$ years. *Note.* The background gradient represents the infection state (normalized) spectrum; color = states (infection with red) \leftarrow \rightarrow (blue) absence of infection).

infectious potential with a probability of $1 - p_p$; $p_p = (p_{p,\max} / (1 + c_{p,1/2} / (f_p c)))$ when an infection lasts for one time step.

Figure 4 presents different observations parameterized by the nonevolutionary macroparameter ($p_{p,\max}$) as the main protection variable with the created matrix of the network (λx = eigenvector centrality). The patterns observed from the four parameterizations provide different evolutionary patterns based on the time series. For small connections (λx low \leftarrow connection $p_k = 0.1$) among individuals, a weakly spreading pattern is observed in which the centralities are widely distributed with strong connections rather than extensive links (λx high \leftarrow connection $p_k = 0.9$) being observed, wherein the centralities are tightly distributed. Furthermore, we see that when the protection thickness is driven, a robust regime emerges in the sense that a sufficient degree of immunity produces a symmetric pattern between the centrality and the protection level and weak protection does not. The results provide insights into the possible patterns available with the artificially designated parameters plausibly being the protective factors against virus diffusion.

3.3. Imposing Rewiring. Even in the observed scenarios that match the disease model, we propose that the contagion is likely to be intensified with a rewiring probability on the nonevolutionary scale (p_β), thereby causing additional infection costs (i.e., mobility and immigration). We determine that intervention provides associated values with the propagation criteria on a macroscale ($p_{p,\max}$) for each node. This observation enables us to gain a sense of the varying nature of propagation within systems. This type of infection is limited to connections and is caused by regulation. Put differently, there is another rate that continues to increase as the protection regime causes cascading infections, even when individuals continue to invest their potential.

Figure 5 represents individuals that differed in their underlying contact rates (p_β), assuming a lower rate from the rewiring interactions among the less vulnerable

simultaneously with their behavioral responses to public nonevolutionary interventions. This shows that the infectiousness differed among individuals even within groups, owing to nonuniform characteristics in the population. We also show that the individuals can vary because of their acceptance, ability, or the availability of a macroscale intervention ($p_{p,\max} = 1$) which seems to protect against propagation.

Furthermore, nodes that are controlled by rewiring seem to maintain their potential only if they can avoid losing their protection, $p_{p,\max} = 1$. We extend this observation until the process properties do not change (i.e., attain stationarity). Hence, they neither increase nor decay, and the process converges to a stationary probability (see Supplementary Materials III for the mathematical mechanism of stationarity).

In terms of stationarity, we observe different levels of protection potential between the parameters ($p_{p,\max}$, p_β) (Figure 6). Thus, to reduce the ramifications of additional losses, a weak connection and rewiring may be preferred to the potential damage (f) from individual infections, but it may guarantee that it is strategically possible for a large insolvent number of individuals to become uninsured connectors (see Supplementary Materials IV for more detail on the mathematical mechanism).

3.4. Part 2: Evolutionary Scale Effect with Recovery. Inspired by COVID-19, to discover the nonevolutionary scale effect underlying the basic reproduction number ($R_t \approx f_n$), we present a network-agent analytical characterization. This is to determine whether an alternative strategy could influence the infection trend that evolves via cultural evolution (i.e., social learning and exploration). We begin this simulation with the assumption that the environment has high protection ($p_{p,\max} = 1$) and moderate centrality (p_k , $p_\beta = 0.25$); however, an agent does (not) have sufficient opportunity to interact with other strategies (f_{p0} and $f_{p1}C$) with values (p_r , $p_e = 0.1$) that reflect the evolutionary microscale that matches the social distance (η)

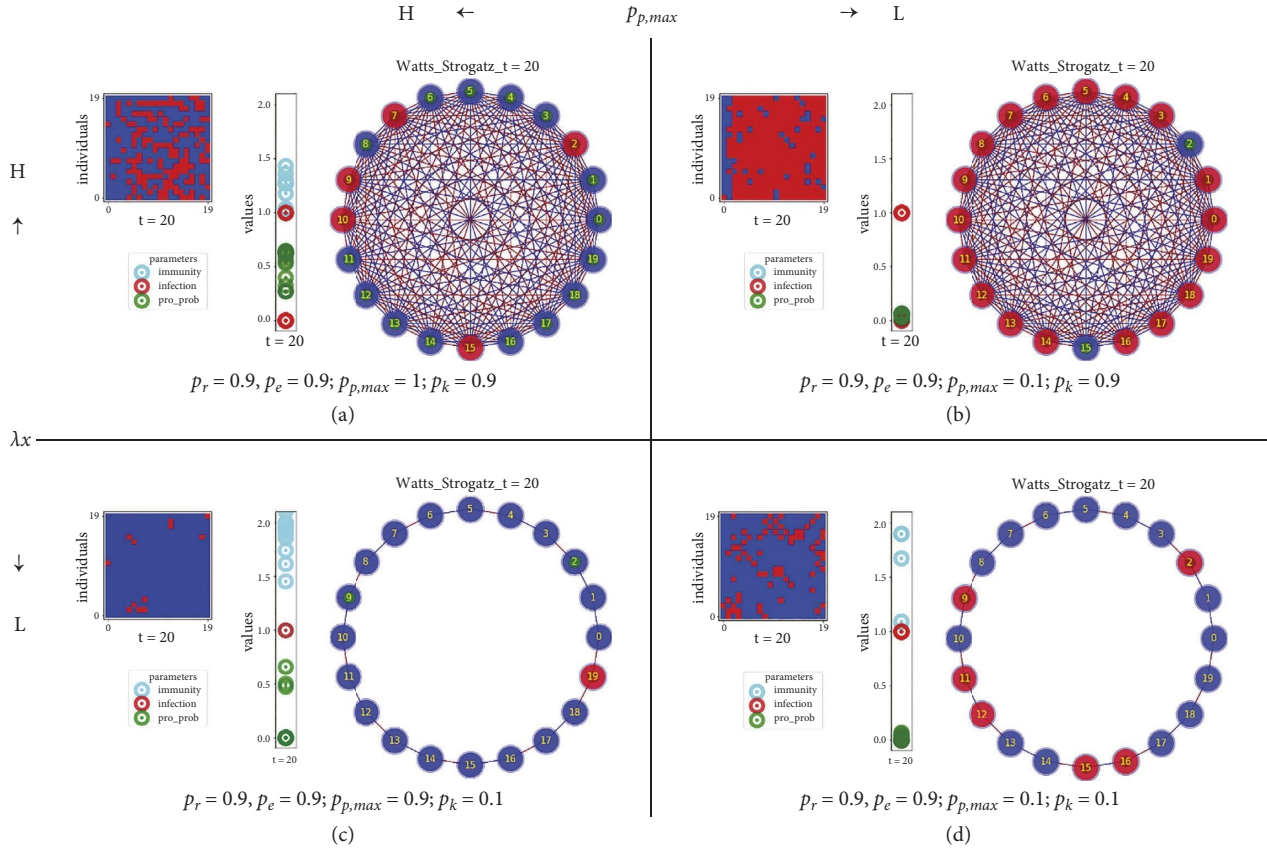


FIGURE 4: Protection dynamics against virus infection. In each section, the plots of the left show the matrix (horizontal axis = time step from 1 to 20; vertical axis = individuals (20); color of the matrix = infection state between infection (red) and absence of infection (blue)). The plots in the middle illustrate each individual's averaged parameter values at the time step ($t = 20$): cyan = immunity; red = infection; green = protection probability). The plot on the right represents individual dynamics within a small-world network; node number = random label of each node; line = edge; node color = states (infection (red) \longleftrightarrow (blue) absence of infection; gray = protection probability (green = initial state); background blue = initial structure of the state without infection and protection). The initialized infectious potentials are $p_n = 0.1$; $p_l = 0.1$.

of the disease model. The imitation and exploration probability causes different protection levels, f_p , according to the virus infection mechanisms:

$$p_p = \frac{P_{p,max}}{1 + (c_{p,1/2}/f_p c)} \leftarrow f_p = f_{p0} + f_{p1} C \leftarrow f_{p0}, f_{p1} C = p_i = [1 + \exp(-\omega \Delta \pi)]^{-1} \leftarrow \sigma_e = f(x|\mu, \sigma^2). \quad (11)$$

The parameter set assumes that different values of $p_r \in [0, 1]$ and $p_e \in [0, 1]$ are incapable of the dynamics, resulting in a given protection level. Hence, even if we set high protections at a macroscale, each agent will (not) choose another as a role model and imitate that agents' strategy values (immunity) at each time step with the applied function ($p_i = [1 + \exp(-s(\pi_r - \pi_f))]^{-1}$). Furthermore, each agent can (rarely) alter its strategic value because there is no opportunity to explore another.

Figures 7 and 8 indicate different strategies for different network infection evolution. As with most real-world

networks, simulation results that use imitation and exploration have parameters that expand nonlinearly over time. The densification suggests that the existing structure may constrain occurrences at the next time step. The evidence indicates that infections between parameters occur during very early stages, demonstrating that the diffusion can be exaggerated by interactions among individuals. Hence, the probability of social learning may be another crucial factor that leads to novel trends having a significant impact on socioeconomic status (see the following mathematical mechanism for more detail).

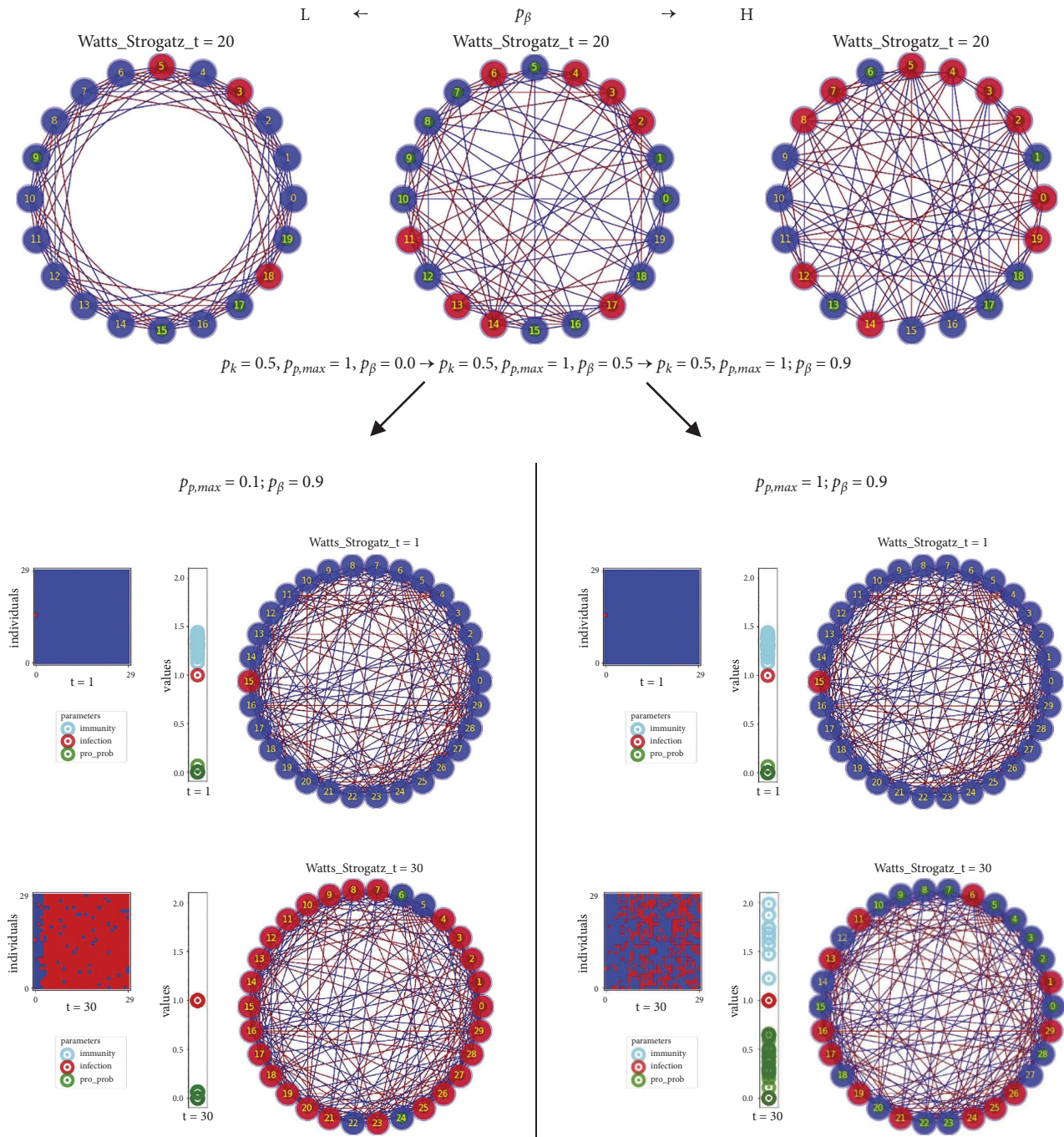


FIGURE 5: A representation of the protection potential constructed by p_β (upper set) and $p_{p,max}$ (bottom set). With the same initialized parameter values ($n = 30$; $p_k = 0.5$; $c_{p,(1/2)} = 0.5$; $p_r = 0.9$; $p_e = 0.9$; and $C = 1$), the set of bottom represents the protection level (left: $p_{p,max} = 0.1$; right: $p_{p,max} = 1$) case. In each section, the plot on the left shows a matrix (horizontal axis = time step from 1 to 30; vertical axis = individuals from 1 to 30; and color of the matrix = infectious state: infection (red) and absence of infection (blue)) corresponding to the parameter values (see legend) of every individual at the given time step. The graph on the right represents their dynamics in a small-world network; node number = random label of each node marked with a blue background; lines = connections embedded by eigenvector centrality as the thickness; and node color = states (infection = red; absence of infection = blue).

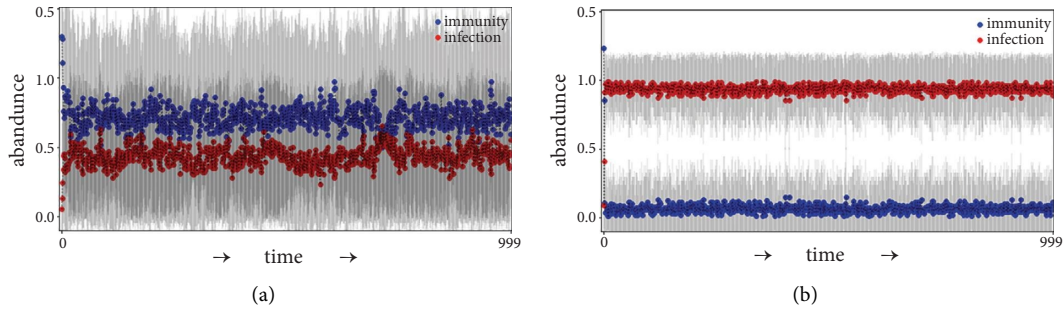


FIGURE 6: Stationarity in time series with small-world graph (nodes = 10×10 ; connection $p = 0.2$; rewiring = 0.5; and time steps = 1,000). The set on the plots shows their extended results ($n = 100$; time steps = 1,000) controlled by the protection maximum with a constant connection and rewiring probability (dots = averaged values; dashed lines = variation). The plot shows infection (red) and immunity (blue) (vertical axis = value corresponding to the time step (horizontal axis) according to the protection maximum ((a) = $[p_{p,max} (0.1)]$, and (b) = $[p_{p,max} (0.9)]$).

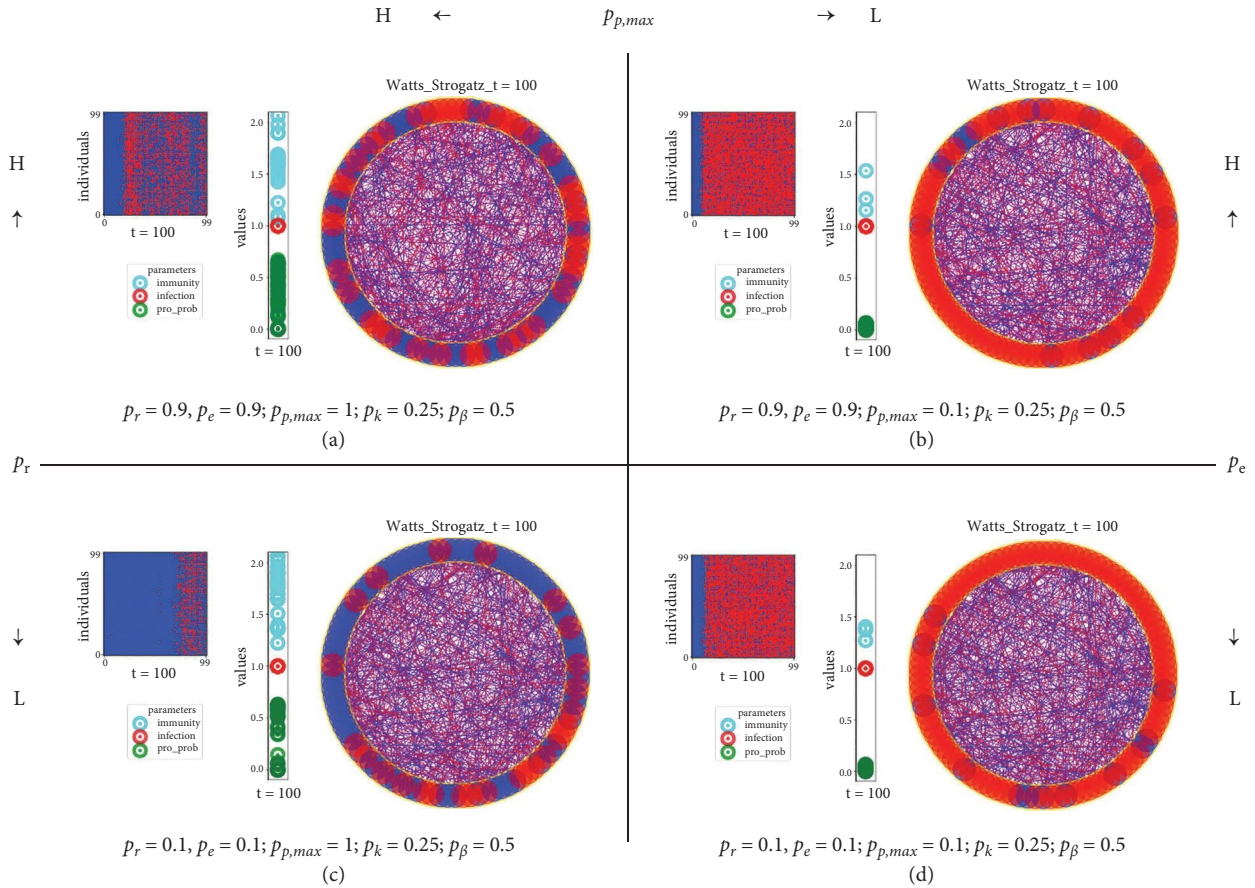


FIGURE 7: Described protection dynamics against virus infection with imitation and exploration rate. In each section, plots of the left show the matrix (horizontal axis = time step from 1 to 100; vertical axis = individuals from 0 to 100; and color of the matrix = infectious state between infected (red) and absence of infected (blue)). The plot on the right represents the individuals' dynamics with a network; node color = states (infection (red) \longleftrightarrow (blue) absence of infection; green = protection potential; and yellow = initial structure of the state without infection and protection). The initialized infectious potentials are $p_n = 0.1$; $p_l = 0.1$.

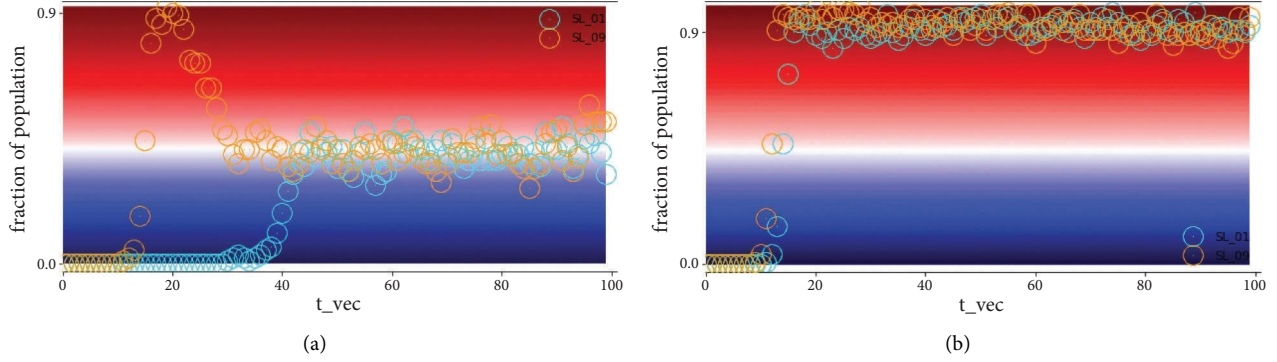


FIGURE 8: Simulation with the intervention scenario parameterized by imitation and exploration (a) with the strong protection maximum ($p_{p,\max} = 1$) and (b) with the weak protection maximum ($p_{p,\max} = 0.1$). Each marker of the plot denotes the averaged (realization = 10) cumulative cases as a fraction of population (orange: imitation and exploration probability (p_r, p_e) = 0.9; cyan: imitation and exploration probability (p_r, p_e) = 0.1). The background gradient represents the infection state dynamics in the entire population (normalized); color = states (infection (red) \longleftrightarrow (blue) absence of infection).

3.4.1. Mathematical Mechanisms of the Evolutionary Microscale Parameter Effect. Let us now consider the numerical insight behind the observation to understand how the evolutionary microscale parameter results can be interpreted. We assume that the applied model is obtained from the most straightforward network algorithm that consists of n inputs and outputs, where n is the number of features of our dataset (i.e., evolutionary parameters). The process of passing data through the network is defined as propagation and is carried out with a systemic risk (virus) as follows.

For the input, multiply the input value \vec{x}_i with the potential \vec{w}_i and sum the multiplied values. The potential corresponding to the model mechanisms is represented by the strength of the interaction (imitation and exploration) protection between individuals, and it is used to determine the extent of the influence that will be assigned to the input on the individual's output. If the potential \vec{w}_1 has a higher value than the potential \vec{w}_2 , input \vec{x}_i will have a more significant influence on the output than \vec{w}_2 .

$$\sum = (\vec{x}_1 \cdot \vec{w}_1) + (\vec{x}_2 \cdot \vec{w}_2) + \dots + (\vec{x}_n \cdot \vec{w}_n). \quad (12)$$

The row vectors of the inputs and potentials are $\vec{x} = [\vec{x}_1, \vec{x}_2, \dots, \vec{x}_n]$ and $\vec{w} = [\vec{w}_1, \vec{w}_2, \dots, \vec{w}_n]$, respectively, and their product is given by

$$\vec{x} \cdot \vec{w} = (\vec{x}_1 \cdot \vec{w}_1) + (\vec{x}_2 \cdot \vec{w}_2) + \dots + (\vec{x}_n \cdot \vec{w}_n). \quad (13)$$

Hence, the summation is equal to the product of vectors x and w :

$$\sum = \vec{x}_i \cdot \vec{w}_i. \quad (14)$$

Next, let us add a risk (virus) b to the summation of the multiplied values, and let us call this expression z . Risk (which is also known as the offset) is necessary to move the entire activation function to the left or right to generate the required output values.

$$z = \vec{x} \cdot \vec{w} + b. \quad (15)$$

Then, we pass the value of z to a nonlinear function as we observed nonlinearity in the individual's output, which is the applied network function. Moreover, the output has a significant effect on the spreading speed of the network in that the network property has a role ($p_i = [1 + \exp(-\omega\Delta\pi)]^{-1}$) as their fundamental mechanism, which is defined here as

$$\hat{y} = \sigma(z) = \frac{1}{(1 + \exp(-z))}, \quad (16)$$

where σ denotes the function, and the output we obtain after the projection is known as the predicted value \hat{y} . This logic comprises an algorithm for computing the rate of change for the potentials. The rate of change is calculated as the square of the difference between the actual (y_i) and predicted (\hat{y}_i) values, which is calculated for the entire dataset, and the average was taken.

$$C = \frac{1}{n} \sum_{i=1}^n (y_i - \hat{y}_i)^2. \quad (17)$$

To find the best potential and risk for our model, we need to determine how the function changes based on potentials and risks. This is achieved with the help of the rate of change. In our case, we need to determine the rate of the function's change with respect to the potential and risk. We calculate the rate of change of the function C for potential w_i using partial differentiation. Because the function (C) is not directly related to the potential w_i , we use the chain rule (probability) as

$$\frac{\partial C}{\partial w_i} = \left(\frac{\partial C}{\partial \hat{y}} \right) \cdot \left(\frac{\partial \hat{y}}{\partial z} \right) \cdot \left(\frac{\partial z}{\partial w_i} \right). \quad (18)$$

To determine the following three rates of changes ($\partial C / \partial \hat{y}$), ($\partial \hat{y} / \partial z$), and ($\partial z / \partial w_i$), we calculate with the rate of change of the function (C) related to the predicted value (\hat{y}).

$$\frac{\partial C}{\partial \hat{y}} = \frac{\partial}{\partial \hat{y}} C, C = \frac{1}{n} \sum_{i=1}^n (y_i - \hat{y}_i)^2 = 2 \cdot \frac{1}{n} \sum_{i=1}^n (y_i - \hat{y}_i). \quad (19)$$

That is, when y = actual vectors and \hat{y} = predicted vectors, the equation is

$$\frac{\partial C}{\partial \hat{y}} = \frac{2}{n} \cdot \sum (y - \hat{y}). \quad (20)$$

$$\frac{\partial}{\partial z} \left[\frac{1}{1 + \exp(-z)} \right] = \frac{\exp(-z)}{1 + \exp(-z)^2} = \frac{1}{1 + \exp(-z)} \cdot \frac{\exp(-z)}{1 + \exp(-z)} = \frac{1}{1 + \exp(-z)} \cdot \left(1 - \frac{1}{1 + \exp(-z)} \right) = \sigma(z) \cdot (1 - \sigma(z)). \quad (22)$$

The rate of change of z to the weight w_i is

$$\frac{\partial z}{\partial w_i} = \frac{\partial}{\partial w_i} (z). \quad (23)$$

Because z equals to $\vec{x} \cdot \vec{w} + b$, it produces

$$\frac{\partial}{\partial w_i} \sum_{i=1}^n (\vec{x}_i \cdot \vec{w}_i + b) = \vec{x}_i. \quad (24)$$

Thus, we get

$$\frac{\partial C}{\partial w_i} = \frac{\partial C}{\partial \hat{y}} \cdot \frac{\partial \hat{y}}{\partial z} \cdot \frac{\partial z}{\partial w_i} = \frac{2}{n} \cdot \sum (y - \hat{y}) \cdot \sigma(z) \cdot (1 - \sigma(z)) \cdot \vec{x}_i. \quad (25)$$

Here, the risk is conceptually considered to have a constant input value of 1. Hence,

$$\frac{\partial C}{\partial b} = \frac{2}{n} \cdot \sum (y - \hat{y}) \cdot \sigma(z) \cdot (1 - \sigma(z)). \quad (26)$$

Finally, we optimize the best element from a set of available alternatives, which, in our case, is the selection of the best potential and risk. Let us select the rate of change descent as our optimization algorithm, which changes the potential and risk, and it is proportional to the negative rate of change of the function C , concerning the corresponding potential or risk. The rate (α) is a hyperparameter used to control the change in the potential and risk. Potential (w_i) and risk (b) are updated as follows, and the rate of change is repeated until we achieve stationarity (divergence or convergence).

$$w_i = w_i - \left(\alpha \cdot \frac{\partial C}{\partial w_i} \right), \quad (27)$$

$$b = b - \left(\alpha \cdot \frac{\partial C}{\partial b} \right).$$

We suggest that this mathematical mechanism behind the simulations is a fundamental concept to obtain all types of results (with some modifications for fitting our model). Despite the logarithmic expansion of our small-world network, if we explore contact individuals or acquaintances in

Now, we find the rate of change of the predicted value for z .

$$\frac{\partial \hat{y}}{\partial z} = \frac{\partial}{\partial z} \sigma(z), \sigma(z) = \frac{1}{(1 + \exp(-z))}. \quad (21)$$

For simplification,

the network, the map of the network creates propagation linked by their connections among neighbors corresponding to the numerical explanations.

3.5. Imposing Recovery. The assessment process was to make macroscale (e.g., institutional competition and central intervention) observations, and microscale (e.g., individual behavior and relative gain) evaluations were simultaneously obtained. To address the central social distancing and isolation intervention methods as confirmed by the simulation, we extended the model to fit an estimation of recovery (microlevel individual immunity recovery) and recovery delays (macrolevel intervention delay), thus obtaining more detailed insights into the network structure.

The simulations displayed in Figure 9 imply that virus diffusion is likely to be intensified by both recovery and recovery time delays (Figure 10), resulting in a significant social cost. We also observe that immediate or delayed temporal interventions (e.g., social distancing, isolation, and quarantining) are associated with micro- and macroscale propagation criteria at each node. The nodes controlled by $t_r = 2$ seem to lose their ability to protect, despite their strong protection level ($p_{p,max} = 1, r_t = 1$). Thus, infections are not limited by protection or strategy (r_t = recovered individuals). However, the rate is affected by regulation over time (t_r = time delay), owing to the propagation of infection. The results having immediate recovery (plots in the left-hand set) appear to have the potential to protect against infection being propagated. Conversely, the results with malfunctions (plots in the right-hand set) do not have this potential, even when the individuals maintain an immune capacity.

3.6. Fit the Network-Agent Dynamic (Evolutionary Microscale Effect) to the Disease Population Dynamic. We suggest that the value depends on three factors. First is the duration of infectiousness of the disease. How long can an infected individual (f_n) cause infections to others? The answer is not simple because this value varies. Infectiousness seems inherently and genetically associated with individuals, and it depends on the state of protection potential (infection)

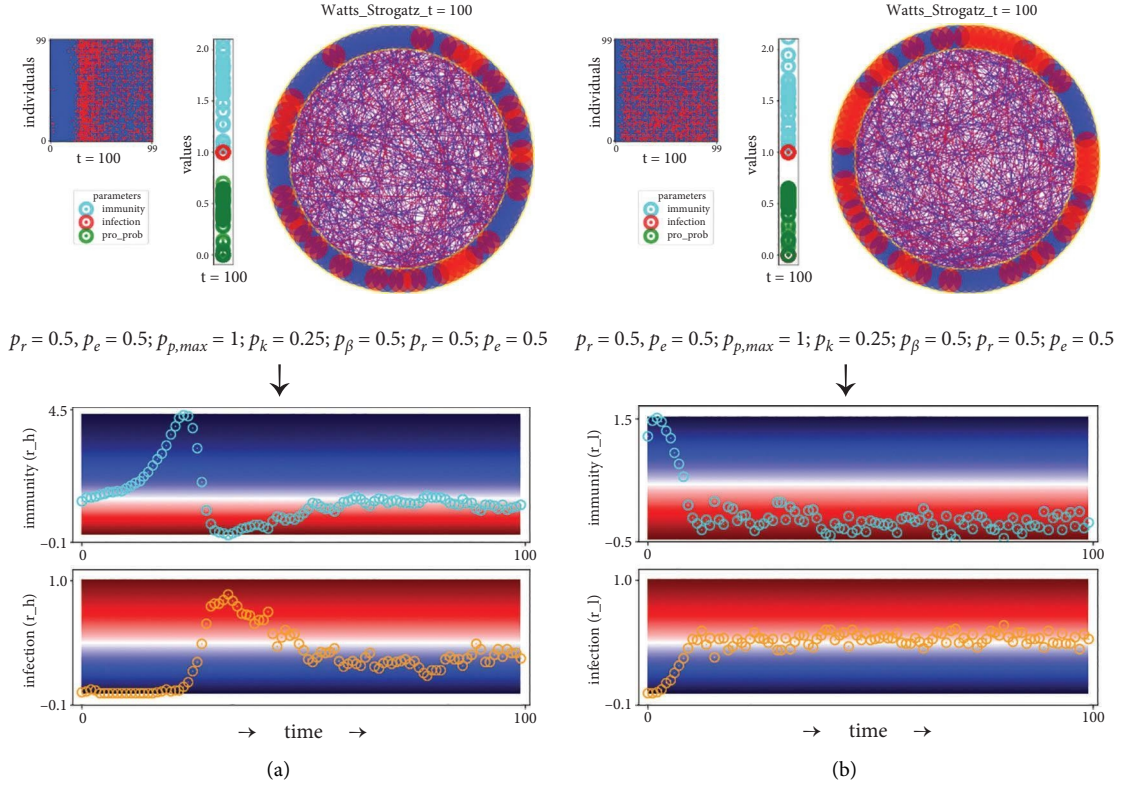


FIGURE 9: Representation of protection potential constructed by recovery rate. With the same initialized parameter values (upper plots: $p_{p,max} = 1$; $c_{p,1/2} = 0.5$; $p_r = 0.5$; $p_e = 0.5$), the set of plots represents the recovery rate (left: $t_r = 1$; right: $t_r < 1$) case. In each section, the plot on the left shows a matrix (horizontal axis = time step from 1 to 100; vertical axis = individuals from 1 to 100; color of the matrix = infectious state: infection (red) and absence of infection (blue)) corresponding to the parameter values of each individual at the given time step. The graph on the right represents their dynamics in a small-world network; node = each individual; lines = connections embedded by eigenvector centrality; node color = states (infection = red; absence of infection = blue). The plots in the bottom sets denote the averaged cumulative cases as a fraction of the population (cyan: immunity; orange: infection). The background contour represents the infection state (normalized) dynamics in the entire population; color = states (infection (red) \longleftrightarrow (blue) absence of infection). (a) Coexistence scenario A: high $p_{p,max}$ and recovery rate $t_r = 1$. (b) Coexistence scenario A: high $p_{p,max}$ and recovery rate $t_r < 1$.

experienced by that individual. At different stages, an influenced individual sheds varying amounts of infectious potential. Second is the probability of infection between infected and susceptible individuals. This depends on the type of contact and the method of propagation. Thus, the reproduction number (R_t) will be different, accounting for virus risk with limited propagation and transmission. The third is the average rate of individual interaction controlled by social interaction (η) between infected and susceptible individuals. This variable depends on the types of structure, interaction, social activities, and so on, in which the individual is involved.

The first two factors are affected by nonevolutionary macroscale characteristics (i.e., regime, governance, and supervision), as determined by the system's centrality. The third is affected by evolutionary microscale characteristics, where activities such as intervention (i.e., social distancing) play a significant role [49]. In Figure 11, we parameterize this rate to allow for an initial period of intense application of intervention measures (i.e., social distancing = η) followed by a relaxation of those measures to enable the socioeconomic activity to resume:

$$\begin{aligned}\beta_{t1} &= \beta_{t,0} \exp(-\eta_1 t) + (1 - \exp(-\eta_1 t))\bar{\beta}_1, \\ \beta_{t2} &= \beta_{t,0} \exp(-\eta_2 t) + (1 - \exp(-\eta_2 t))\bar{\beta}_2;\end{aligned}\quad (28)$$

therefore,

$$\beta_t = \frac{(\beta_{1t} + \beta_{2t})}{2}. \quad (29)$$

Here, $\beta_0 = ((\beta_{1,0} + \beta_{2,0})/2)$ denotes the initial value of β_t , which represents the spread of the virus during its initial phase. The parameters $\bar{\beta}_i$ for $i = 1, 2$ indicate that the long-run values of β_{1t} converge. Thus, eventually, β_t converges to $((\bar{\beta}_1 + \bar{\beta}_2)/2)$. To obtain a U-shaped pattern for β_t , we make β_{1t} a rapidly declining function and β_{2t} a slowly rising function. The parameter η_1 governs the rate at which β_{1t} infects $\bar{\beta}_1$. The parameter η_2 governs the rate at which β_{2t} rises towards $\bar{\beta}_2$. For each simulation, we obtained slightly different results, which allowed us to provide mitigating scale parameters.

We performed the simulation to obtain the image shown in Figure 11. From the simulations, we can detect the effects of various types of interventions (i.e., distancing

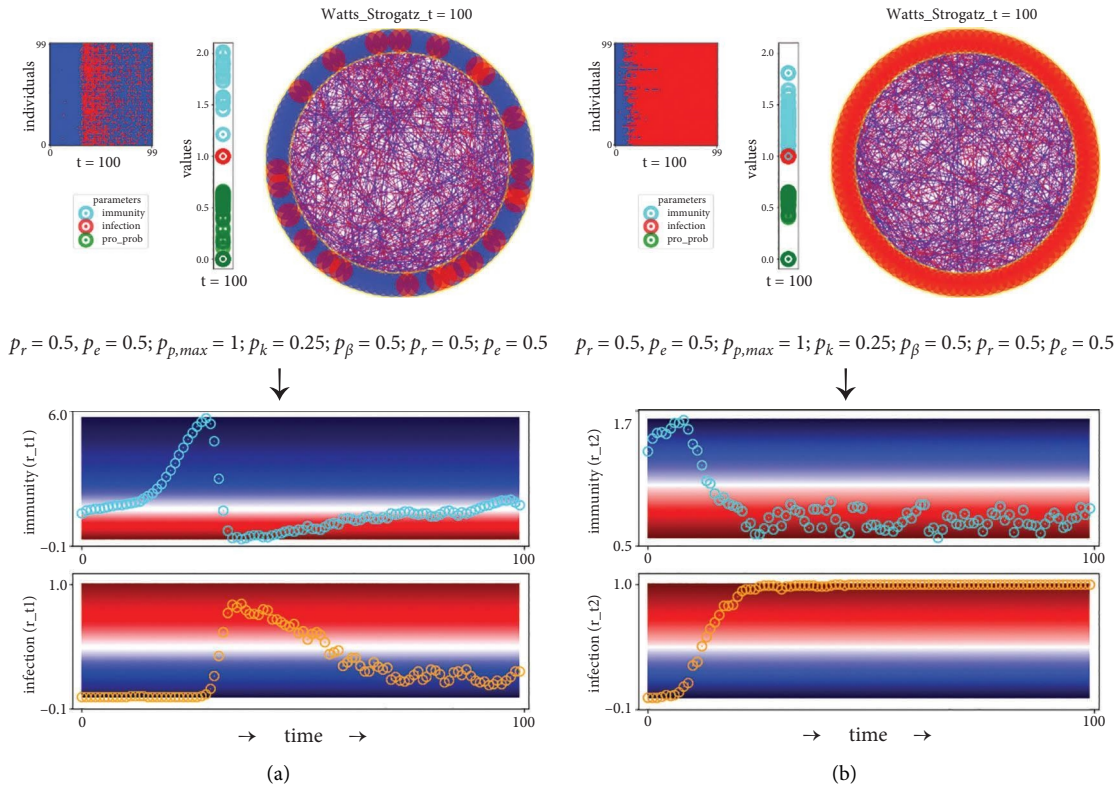


FIGURE 10: Representation of protection potential constructed by recovery time delay. With the same initialized parameter values (upper plots: $p_{p,max} = 1$; $c_{p,1/2} = 0.5$; $p_r = 0.5$; $p_e = 0.5$), the set of plots represents the recovery time delay (left: $r_t = 1$; right: $r_t = 2$) case. In each section, the left plots show a matrix (horizontal axis = time step from 1 to 100; vertical axis = individuals from 1 to 100; the color of the matrix = infectious state: infection (red) and absence of infection (blue)) corresponding to the parameter values of each individual at the given time step. The right graphs represent their dynamics in a small-world network; node = each individual; lines = connections embedded by eigenvector centrality; node color = states (infection = red; absence of infection = blue). The plot of the bottom sets denotes the averaged cumulative cases as a fraction of the population (cyan: immunity; orange: infection). The background gradient represents the infection state (normalized) dynamics in the entire population; color = states (infection (red) \longleftrightarrow (blue) absence of infection). (a) Coexistence scenario A: high $p_{p,max}$ and delay $r_t = 1$. (b) Coexistence scenario A: high $p_{p,max}$ and delay $r_t = 2$.

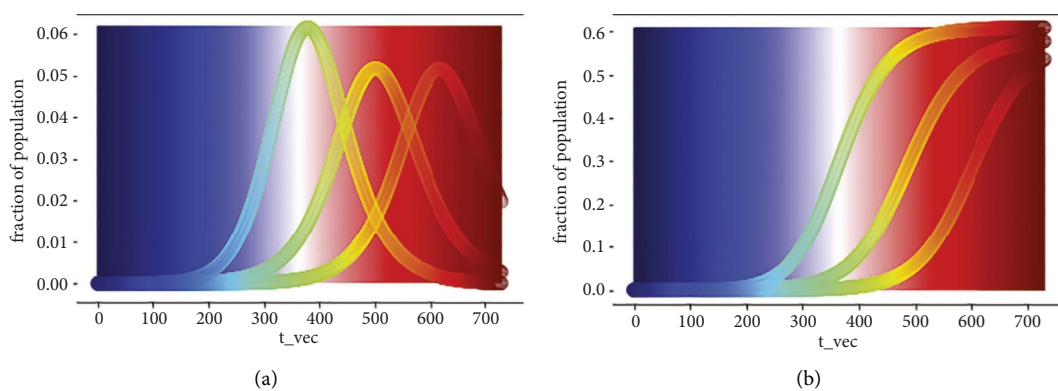


FIGURE 11: Comparison with the intervention scenario parameterized by social distancing (η) and social learning = p_r, p_e . (a) The fraction of the population (left: $\eta = 0.1$; middle: $\eta = 0.5$; right: $\eta = 0.9$) produced by the population dynamic model. (b) The cumulative cases as a fraction of the population (left: infectious potential (f_n) = high \longleftrightarrow right: infectious potential (f_n) = low) produced by the network-agent social learning dynamic (p_r, p_e ; left: $p_r, p_e = 0.9$; middle: $p_r, p_e = 0.5$; right: $p_r, p_e = 0.1$). The background gradient represents the infection state (normalized) spectrum; color = states (infection (red) \longleftrightarrow (blue) absence of infection).

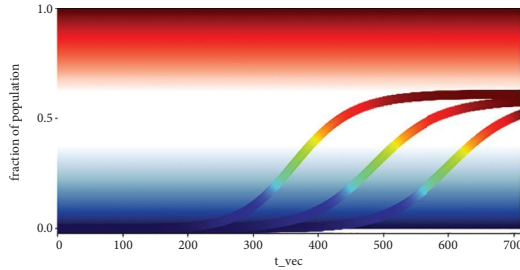


FIGURE 12: Schematic representation of the final intervention scenario parameterized by the evolutionary interactions ($= f_p C$). The plot represents intervention outcomes (i.e., intervention outcomes when the transition rate equals three). Each line of the plot denotes the cumulative cases as a fraction of the population (left: mild, middle: moderate, and right: extensive), time step $t = 2$ years.

and social learning) on the number of cases and how they change over time. Thus, we have states of infection, absence of infection, and recovery, in a free-for-all attempted intervention (i.e., quarantine, moderate distancing, and extensive distancing).

4. Discussion

The proposed infection probability model was created to run with many simulations based on the time steps of virus risk propagation throughout the network and eventually provide the final number of infections. The results indicate that individuals are more affected when they are highly linked to the network [49]. Thus, the probability of infection is determined by the number of connections and the rewiring from the node of the specification scaled at the macrolevel. The rationale behind these observations is that higher-degree agents are more exposed to infection than lower-degree ones, which increases the potential for cascading [50].

From these observations, we attempted to identify what stabilizes the propagation rate. In this regard, we know that there are delays in requesting and receiving tests, obtaining disease results, and sending the results to health authorities [51]. We have a variable $\beta_t = p_l$ that reflects the potential of infection in a designated population. Meanwhile, the variable is not constant in each trial, owing to interventions, which are (not) made up of (in)dependent trials [52]. In our results, this trend is observed in the model's (non)evolutionary macro/microscale parameters. However, their influences are not identically weighted [53]. The intervention applied to the risk potential can persist briefly, and we can cite this as a virus infection. Thus, to reduce the potential ramifications ($R_t = (f_n)$), interconnected and immediate interventions are preferred to determine the potential damage from individual infections to guarantee that a strategy to recover from losses to uninsured connectors is possible [54].

Inspired by the plausible scenarios presented above, we focused on the evolutionary parameter ($f_p c$) having a more individualized perspective with time steps. The results yield the important insight that weakly centralized regimes

allowing high numbers of interactions among individuals should not be recommended [55] in the current model. Moreover, we should shift away from the extant dominant potentials, norms, and routines that can lead to novel trends that have a high impact (Figure 12).

The evidence shows that strictly confined individual movements are key to diffusion and that contagions occur at early stages (see Figure 8). Hence, individual interaction (e.g., social distancing) probabilities and rates are crucial factors that lead to violated expectations and novel trends having a high impact [56]. Following these observations, we can assume that successful outcomes require a delicate balance across these essential components (macro- and microscale). Individuals and organizations may find value in reducing their perceived virus risk potential by following this suggestion. Although many questions remain regarding how other network structures, governance schemes, and content evolve and interact over time and new COVID variants, resources should be used to help gauge the underlying potential. The observations from our simulations may lead to beneficial network structures and connectivity supported by joint governance [57].

This interpretation helps estimate how countries have tackled the pandemic by connecting the governmental-individual levels of effort. For example, some countries responded swiftly to initial cases [45]. They rolled out a “test, trace, and track (3T)” approach, fast-tracked the mass production of test kits, and set up drive-thru and walk-in test centers (i.e., robust macroscale parameters) that provided results within 24 h. They tested many people per day (i.e., $\sim 20,000$), globally the highest at that time [58]. In the early cases, the authorities attempted to trace everyone who had encountered infected individuals and tested them to prevent the virus from spreading. Those who were confirmed positive were asked to isolate themselves voluntarily (weak microscale interaction) and to download an app that alerted authorities if they left their home. People in the vicinity of an infected individual also received alerts (i.e., phone) from the government. This testing approach allowed the government to avoid a nationwide lockdown; however, large public gatherings were banned, and schools were shut down.

At the macroscale, all arrivals into the country should be quarantined (i.e., for two weeks). Countries that did this contained the virus' early spread [59]. Hence, for all positive tests, their government should test and trace all contacts to break the transmission chain. Furthermore, countries should prepare contact-tracing measures. Laws should be adapted to allow the government to collect patient data and security footage during an outbreak to increase their macroscale intervention [60]. At the microscale, all steps should be logged and shared to alert people to avoid the path to infection (i.e., decrease the number of connections). Websites and private apps could compile this information to allow everyone to see where infected persons are or have been and when. Citizens should actively check and avoid locales of infection. Such microlevel voluntary efforts would be extremely helpful in controlling the spread. Tracing

people's movements is often considered controversial; however, governments should prioritize public safety over privacy during an outbreak [61].

Such efforts will allow countries to test hundreds of thousands of people quickly and effectively, thereby making it easier to contain the virus. By doing so, aggressive lockdowns could be avoided. Furthermore, it would proactively help flatten the outbreak curve from steep to level. Currently, the world has turned a corner in the pandemic; however, we must continue to be prepared. Levels of vigilance have set some countries apart [62] who, in this manner, demonstrated the benefits of widespread testing [63]. More testing is required, but aggressive strategies may be difficult to implement in countries with much larger populations.

5. Conclusion

Contagions and persistence patterns should not be viewed as having causal links; rather, they should be seen as driven by interconnectedness [64]. The potential is caused by macro- and microscale parameters [65]. Delayed response times cause increased risk propagation, which is likely to allow widespread infections, thus leading to reductions in network (social) welfare. Governance and personal misbehavior (e.g., under- or overestimating the situation) may, at times, stretch to many networks, thus increasing the risk [66]. Given that the evolutionary mechanisms implemented in this simulation model match the real disease model, we often observed evolutionary responses to obtain a critical value for a plausible protection potential [67]. Although the structures have high infectious potential in terms of virus risk, the interconnected macroscale-microscale intervention measures become weak amplifiers as protection increases [68].

According to the World Health Organization (2020), the COVID-19 pandemic and the associated economic crisis pose huge global and local challenges. The health, social, and economic impacts have affected all segments of the population; however, it is particularly detrimental to vulnerable social groups, including people living in poverty, older persons, persons with disabilities, and Indigenous peoples. Epidemics and economic crises have a disproportionate impact on these vulnerable groups, which can trigger worsening inequality and poverty. The global crisis requires the coordination of stakeholders, a global solution, local implementation of effective socioeconomic and public health policies, and solidarity [69]. The idea is simultaneously to starve the virus everywhere through a combination of quarantine, social distancing, and restricted travel. The critical factor is the synchronization of responses [70]. In a typical pandemic, when one country peaks, another may be observing its first cases (even variants). Instead of leaders responding only to what is happening in their jurisdictions, the world should be treated as a giant interconnected system. If coordinated properly, global efforts can quickly end such pandemics, thus ensuring reduced loss of life. However, unless the virus is completely eradicated, which is highly unlikely, propagation risks will persist [71].

Thus, finding a global response strategy for the pandemic is key. Breakthroughs in the treatment and prevention of symptoms can also make viruses far less dangerous while requiring fewer extreme containment measures [72]. Ultimately, the breakthroughs, social services, and systems we develop can be used for a better future for everyone.

Data Availability

The data used to support the findings of this study are included in the article.

Ethical Approval

This study was approved by the local ethics committee (SNUIRB No. 1509/002-002), conforming to the ethical standards of the 1964 Declaration of Helsinki (Collaborative Institutional Training Initiative Program, report ID 20481572).

Consent

All participants in the study provided written informed consent.

Conflicts of Interest

The author declares that there are no conflicts of interest regarding the publication of this paper.

Acknowledgments

The author wishes to thank Åke Brännström at International Institute for Applied Systems Analysis (Austria), Henrik Sjödin at Public Health and Clinical Medicine Umeå University (Sweden), and Seung Ki Baek at Statistical Physics Pukyong National University (South Korea) for their fruitful discussion during the development of this paper. This research was supported by the Basic Science Research Program through the National Research Foundation of Korea funded by the Ministry of Education (Grant no. 2020R111A1A01056967) (PI: Chulwook Park). This work was also supported under the Framework of International Cooperation Program managed by the National Research Foundation of Korea (Grant no. 2021K2A9A1A0110218711) (PI: Chulwook Park).

Supplementary Materials

Supplementary file includes model mechanisms and parameter calculation. (I) Mathematical mechanism of the basic network property. (II) The SEIR model mechanism. (III) Mathematical mechanism of Stationarity. (IV) Mathematical mechanisms of the nonevolutionary macroscale parameter effect. Supplementary Materials (*Supplementary Materials*)

References

- [1] M. Haire, "Biological models and empirical histories of the growth of organizations," *Mod. Org. Theor.*, vol. 10, pp. 272–306, 1959.
- [2] R. Hagedorn, "Statistical thermodynamics of strong interactions at high energies," *Nuovo Cimento A*, vol. 3, no. 520, pp. 147–186, 1965.

- [3] J. Thachil, N. Tang, S. Gando et al., "ISTH interim guidance on recognition and management of coagulopathy in COVID-19," *Journal of Thrombosis and Haemostasis*, vol. 18, no. 5, pp. 1023–1026, 2020.
- [4] P. J. Schweizer and R. Renn, "Governance of systemic risks for disaster prevention and mitigation," *Disaster Prevention and Management*, vol. 28, 2019.
- [5] N. Beale, D. G. Rand, H. Battey, K. Croxson, R. M. May, and M. A. Nowak, "Individual versus systemic risk and the regulator's dilemma," *Proceedings of the National Academy of Sciences*, vol. 108, no. 31, Article ID 12647, 2011.
- [6] F. Caccioli, P. Barucca, and T. Kobayashi, "Network models of financial systemic risk: a review," *Journal of Computational Social Science*, vol. 1, no. 1, pp. 81–114, 2018.
- [7] S. Pahwa, C. Scoglio, and A. Scala, "Abruptness of cascade failures in power grids," *Scientific Reports*, vol. 4, no. 1, p. 3694, 2014.
- [8] S. Sahasrabudhe and A. E. Motter, "Rescuing ecosystems from extinction cascades through compensatory perturbations," *Nature Communications*, vol. 2, no. 1, pp. 170–178, 2011.
- [9] A. B. Hogan, B. L. Jewell, E. Sherrard-Smith et al., "Potential impact of the COVID-19 pandemic on HIV, tuberculosis, and malaria in low-income and middle-income countries: a modelling study," *Lancet Global Health*, vol. 8, no. 9, Article ID e1132, 2020.
- [10] J. Jia, J. Ding, S. Liu et al., "Modeling the Control of COVID-19: Impact of Policy Interventions and Meteorological Factors," *Electronic Journal of Differential Equations*, vol. 2020, 2020.
- [11] S. Mendolia, O. Stavrunova, and O. Yerokhin, "Determinants of the Community Mobility during the Covid-19 Epidemic: The Role of Government Regulations and Information," *Journal of Economic Behavior & Organization*, vol. 184, 2020.
- [12] R. McGregor, A. L. Whitcombe, C. R. Sheen et al., "Collaborative networks enable the rapid establishment of serological assays for SARS-CoV-2 during nationwide lockdown in New Zealand," *PeerJ*, vol. 8, Article ID e9863, 2020.
- [13] O. Coibion, Y. Gorodnichenko, and M. Weber, "The cost of the covid-19 crisis: Lockdowns, macroeconomic expectations, and consumer spending," National Bureau of Economic Research, Cambridge, MA, USA, No. w27141, 2020.
- [14] J. Wise, "Covid-19: risk of second wave is very real, say researchers," *BMJ: British Medical Journal*, vol. 369, 2020.
- [15] D. O'Sullivan, M. Gahegan, D. J. Exeter, and B. Adams, "Spatially explicit models for exploring COVID-19 lockdown strategies," *Transactions in GIS*, vol. 24, no. 4, pp. 967–1000, 2020.
- [16] M. Nicola, Z. Alsafi, C. Sohrabi et al., "The socio-economic implications of the coronavirus pandemic (COVID-19): a review," *International Journal of Surgery*, vol. 78, pp. 185–193, 2020.
- [17] K. O. Kwok, F. Lai, W. I. Wei, S. Y. S. Wong, and J. W. T. Tang, "Herd immunity—estimating the level required to halt the COVID-19 epidemics in affected countries," *Journal of Infection*, vol. 80, no. 6, pp. e32–e33, 2020.
- [18] A. Fontanet and S. Cauchemez, "COVID-19 herd immunity: where are we?" *Nature Reviews Immunology*, vol. 20, no. 10, pp. 583–584, 2020.
- [19] T. Britton, F. Ball, and P. Trapman, "A mathematical model reveals the influence of population heterogeneity on herd immunity to SARS-CoV-2," *Science*, vol. 369, no. 6505, pp. 846–849, 2020.
- [20] M. Brisson, É. Bénard, M. Drolet et al., "Population-level impact, herd immunity, and elimination after human papillomavirus vaccination: a systematic review and meta-analysis of predictions from transmission-dynamic models," *The Lancet Public Health*, vol. 1, no. 1, pp. e8–e17, 2016.
- [21] G. Giordano, F. Blanchini, R. Bruno et al., "Modelling the COVID-19 epidemic and implementation of population-wide interventions in Italy," *Nature Medicine (New York, NY, United States)*, vol. 1–6, 2020.
- [22] L. Peeples, "Avoiding pitfalls in the pursuit of a COVID-19 vaccine," *Proceedings of the National Academy of Sciences*, vol. 117, no. 15, pp. 8218–8221, 2020.
- [23] M. Roser, H. Ritchie, E. Ortiz-Ospina, and J. Hasell, "Coronavirus pandemic (COVID-19)," *Our World in Data*, vol. 4, 2020.
- [24] N. Lurie, M. Saville, R. Hatchett, and J. Halton, "Developing Covid-19 vaccines at pandemic speed," *New England Journal of Medicine*, vol. 382, no. 21, pp. 1969–1973, 2020.
- [25] J. J. Van Bavel, K. Baicker, P. S. Boggio et al., "Using social and behavioural science to support COVID-19 pandemic response," *Nature Human Behaviour*, vol. 1–12, 2020.
- [26] C. Pawlowski, A. Puranik, H. Bandi et al., "Exploratory analysis of immunization records highlights decreased SARS-CoV-2 rates in individuals with recent non-COVID-19 vaccinations," *Scientific Reports*, vol. 11, no. 1, pp. 1–20, 2021.
- [27] K. Tyagi, A. Ghosh, D. Nair et al., "Breakthrough COVID19 infections after vaccinations in healthcare and other workers in a chronic care medical facility in New Delhi, India," *Diabetes & Metabolic Syndrome: Clinical Research Reviews*, vol. 15, no. 3, pp. 1007–1008, 2021.
- [28] K. N. Laland, "Social learning strategies," *Animal Learning & Behavior*, vol. 32, no. 1, pp. 4–14, 2004.
- [29] M. A. Di Muro, C. E. La Rocca, H. E. Stanley, S. Havlin, and L. A. Braunstein, "Recovery of interdependent networks," *Scientific Reports*, vol. 6, no. 1, Article ID 22834, 2016.
- [30] E. Bonabeau, "Agent-based modeling: methods and techniques for simulating human systems," *Proceedings of the National Academy of Sciences*, vol. 99, no. 3, pp. 7280–7287, 2002.
- [31] A. Vespignani, "Twenty years of network science," *Nature*, vol. 528–529, 2018.
- [32] J. M. Pacheco, A. Traulsen, and M. A. Nowak, "Coevolution of strategy and structure in complex networks with dynamical linking," *Physical Review Letters*, vol. 97, no. 25, Article ID 258103, 2006.
- [33] M. O. Jackson and L. Yariv, "Diffusion of behavior and equilibrium properties in network games," *The American Economic Review*, vol. 97, no. 2, pp. 92–98, 2007.
- [34] M. O. Jackson, B. W. Rogers, and Y. Zenou, "The economic consequences of social-network structure," *Journal of Economic Literature*, vol. 55, no. 1, pp. 49–95, 2017.
- [35] G. Capano, M. Howlett, D. S. L. Jarvis, M. Ramesh, and N. Goyal, "Mobilizing policy (In)Capacity to fight COVID-19: understanding variations in state responses," *Policy and Society*, vol. 39, no. 3, pp. 285–308, 2020.
- [36] Y. Toyoshima, K. Nemoto, S. Matsumoto, Y. Nakamura, and K. Kiyotani, "SARS-CoV-2 genomic variations associated with mortality rate of COVID-19," *Journal of Human Genetics*, vol. 65, no. 12, pp. 1075–1082, 2020.
- [37] J. Mezei and P. Sarlin, "Aggregating expert knowledge for the measurement of systemic risk," *Decision Support Systems*, vol. 88, pp. 38–50, 2016.
- [38] R. Albert, "Emergence of scaling in random networks," *Science (New York, N.Y.)*, vol. 286, no. 5439, pp. 509–512, 1999.
- [39] O. Sporns, D. Chialvo, M. Kaiser, and C. Hilgetag, "Organization, development and function of complex brain

- networks,” *Trends in Cognitive Sciences*, vol. 8, no. 9, pp. 418–425, 2004.
- [40] M. Lelarge and J. Bolot, “A local mean field analysis of security investments in networks,” in *Proceedings of the 3rd international workshop on Economics of networked systems*, vol. 25–30, San Diego, CA, USA, March 2008.
- [41] M. E. J. Newman, “The structure and function of complex networks,” *SIAM Review*, vol. 45, no. 2, pp. 167–256, 2003.
- [42] M. Barthélemy and L. A. Nunes Amaral, “Small-world networks: evidence for a crossover picture,” *Physical Review Letters*, vol. 82, no. 15, p. 3180, 1999.
- [43] D. J. Watts and S. H. Strogatz, “Collective dynamics of ‘small-world’ networks,” *Nature*, vol. 393, no. 6684, pp. 440–442, 1998.
- [44] J. S. Weitz, S. J. Beckett, A. R. Coenen et al., “Modeling shield immunity to reduce COVID-19 epidemic spread,” *Nature Medicine*, vol. 26, no. 6, pp. 849–854, 2020.
- [45] Y. J. Park, Y. J. Choe, O. Park et al., “Contact tracing during coronavirus disease outbreak, South Korea, 2020,” *Emerging Infectious Diseases*, vol. 26, no. 10, pp. 2465–2468, 2020.
- [46] A. Atkeson, “What Will Be the Economic Impact of COVID-19 in the US? Rough Estimates of Disease Scenarios,” National Bureau of Economic Research, Cambridge, MA, USA, No. w26867, 2020.
- [47] M. Park, A. R. Cook, J. T. Lim, Y. Sun, and B. L. Dickens, “A systematic review of COVID-19 epidemiology based on current evidence,” *Journal of Clinical Medicine*, vol. 9, no. 4, p. 967, 2020.
- [48] J. O. Lloyd-Smith, S. J. Schreiber, P. E. Kopp, and W. M. Getz, “Superspreading and the effect of individual variation on disease emergence,” *Nature*, vol. 438, no. 7066, pp. 355–359, 2005.
- [49] E. Klarreich, “Scant evidence of power laws found in real-world networks,” *Quanta Mag*, Article ID 20180215, 2018.
- [50] C. Park, “Network and Agent Dynamics with Evolving Protection against Systemic Risk,” *Complexity*, vol. 2020, Article ID 2989242, 16 pages, 2020.
- [51] A. Resulaj, R. Kiani, D. M. Wolpert, and M. N. Shadlen, “Changes of mind in decision-making,” *Nature*, vol. 461, no. 7261, pp. 263–266, 2009.
- [52] M. A. Croon and M. J. P. M. van Veldhoven, “Predicting group-level outcome variables from variables measured at the individual level: a latent variable multilevel model,” *Psychological Methods*, vol. 12, no. 1, pp. 45–57, 2007.
- [53] R. B. Duffey, “The Quantification of Systemic Risk and Stability: New Methods and Measures,” National Bureau of Economic Research, Cambridge, MA, USA, No. W17022, 2011.
- [54] P. Lange and G. Garrett, “The politics of growth: strategic interaction and economic performance in the advanced industrial democracies, 1974-1980,” *The Journal of Politics*, vol. 47, no. 3, pp. 792–827, 1985.
- [55] C. Van den Bulte and G. L. Lilien, “Bias and systematic change in the parameter estimates of macro-level diffusion models,” *Marketing Science*, vol. 16, no. 4, pp. 338–353, 1997.
- [56] B. Kogut, “The network as knowledge: generative rules and the emergence of structure,” *Strategic Management Journal*, vol. 21, no. 3, pp. 405–425, 2000.
- [57] J. H. Tanne, E. Hayasaki, M. Zastrow, P. Pulla, P. Smith, and A. G. Rada, “COVID-19: how doctors and healthcare systems are tackling coronavirus worldwide,” *BMJ*, vol. 368, Article ID m1090, 2020.
- [58] J.-Y. Song, J.-G. Yun, J.-Y. Noh, H.-J. Cheong, and W.-J. Kim, “Covid-19 in South Korea - csm,” *New England Journal of Medicine*, vol. 382, no. 19, pp. 1858–1859, 2020.
- [59] E. Shim, A. Tariq, W. Choi, Y. Lee, and G. Chowell, “Transmission potential and severity of COVID-19 in South Korea,” *International Journal of Infectious Diseases*, 2020.
- [60] S. Park, G. J. Choi, and H. Ko, “Information Technology-Based Tracing Strategy in Response to COVID-19 in South Korea—privacy Controversies,” *JAMA The Journal of the American Medical Association*, vol. 323, 2020.
- [61] A. S. Arora, H. Rajput, and R. Changotra, “Current perspective of COVID-19 spread across South Korea: exploratory data analysis and containment of the pandemic,” *Environment, Development and Sustainability*, vol. 1–11, 2020.
- [62] J. Oh, J. K. Lee, D. Schwarz, H. L. Ratcliffe, J. F. Markuns, and L. R. Hirschhorn, “National response to COVID-19 in the Republic of Korea and lessons learned for other countries,” *Health Sys*, *Reforma*, vol. 6, no. 1, Article ID 1753464, 2020.
- [63] B. D. Jones, “Behavioral rationality as a foundation for public policy studies,” *Cognitive Systems Research*, vol. 43, pp. 63–75, 2017.
- [64] M. Sampath, R. Sengupta, S. Lafortune, K. Sinnamohideen, and D. C. Teneketzis, “Failure diagnosis using discrete-event models,” *IEEE Transactions on Control Systems Technology*, vol. 4, no. 2, pp. 105–124, 1996.
- [65] J. Lorenz, S. Battiston, and F. Schweitzer, “Systemic risk in a unifying framework for cascading processes on networks,” *The European Physical Journal B*, vol. 71, no. 4, pp. 441–460, 2009.
- [66] M. McKee and D. Stuckler, “If the world fails to protect the economy, COVID-19 will damage health not just now but also in the future,” *Nature Medicine*, vol. 26, no. 5, pp. 640–642, 2020.
- [67] G. Mboowa, “Current and emerging diagnostic tests available for the novel COVID-19 global pandemic,” *AAS open research*, vol. 3, p. 8, 2020.
- [68] World Health Organization, “Coronavirus disease 2019 (COVID-19): situation report,” *Weekly Epidemiological and Operational updates*, vol. 82, 2020.
- [69] S. E. Johnson, M. C. Libicki, and G. F. Treverton, *New Challenges, New Tools for Defense Decision Making*, Rand Corporation, Santa Monica, CA, USA, 2003.
- [70] S. H. Ebrahim, J. Zhuo, E. Gozzer et al., “All hands on deck: a synchronized whole-of-world approach for COVID-19 mitigation,” *International Journal of Infectious Diseases*, vol. 98, pp. 208–215, 2020.
- [71] S. Neumann-Böhme, N. E. Varghese, I. Sabat et al., “Once we have it, will we use it? A European survey on willingness to be vaccinated against COVID-19,” *The European Journal of Health Economics*, vol. 1–6, 2020.
- [72] C. Park, “Role of Recovery in Evolving Protection against Systemic Risk: A Mechanical Perspective in Network-Agent Dynamics,” *Complexity*, vol. 2021, Article ID 4805404, 23 pages, 2021.